The Effect of Various Additions on the Oxidation Behavior of the γ/γ′ Ni-Based Alloy

Jarosław Dąbek[1] · Janusz Prażuch[1] · Monika Migdalska[1] · Monika Jawańska[1] · Magdalena Ziąbka[1] · Monika Wójcik-Bania[2] · Jerzy Jedliński[1]

Abstract

The oxidation behavior of four γ/γ′ Ni-based alloys: without additions, and containing: Hf (1.0 wt%), a combination of Hf and Y (0.3 wt% and 0.03 wt%, respectively), and a combination of Hf and Si (1.0 wt% and 1.0 wt%, respectively) was studied in air under isothermal (50 h) and thermal cycling (up to 2225 1-h cycles) conditions. Samples were characterized using SEM, EDX and XRD techniques. The results indicated that all the additions improved the oxidation resistance of the alloy but only in the case of materials containing the (Hf + Y) combination of additions was a long-term effect achieved. Substantial weight losses were observed on the other unmodified and (Hf + Si)-containing materials during thermal cycling after short exposure periods, while on material containing only additions of Hf, they occurred significantly later. Kinetic studies showed the highest oxidation rate in the case of the (Hf + Si)-containing alloys and the fastest initial oxidation, prior to the parabolic law-obeying stage, of alloy with Hf-additions, only. The results indicate the superior effect of simultaneous application of Hf and Y additions at levels not exceeding their solubility limits and that lowering its effectiveness Hf overdoping (1 wt%) cannot be effectively counteracted by the addition of 1% Si.

Keywords γ/γ′ Ni-based alloys · High-temperature oxidation · Hafnium · Yttrium and/or silicon additions

Introduction

The two-phase γ/γ′ Ni–Al-based alloys, mostly γ/γ′-type ones, alloys that usually contain also Pt, are considered as promising high-temperature coating materials [1–20]. Their oxidation resistance can be improved by additions of reactive elements

✉ Jerzy Jedliński
jedlinsk@agh.edu.pl

Extended author information available on the last page of the article

Table 1 Actual composition of the studied alloys (in wt%)

Alloy	Ni	Al	Hf	Y	Si
γ0	Bal	13.0	–	–	–
γHf	Bal	12.5	1.09	–	–
γHfY	Bal	12.7	0.26	0.024	–
γHfSi	Bal	12.6	0.93	–	1.05

(e.g., Hf, Y), due to the well-evidenced, so-called, reactive-element-effect, reviewed elsewhere [21–23], while the effect of silicon additions is still under investigation [11, 14, 17]. However, in order to optimize the beneficial effect of the reactive elements in qualitative and quantitative terms, as well as to examine the effect of Si, the oxidation behavior should be elucidated as a function of the additions (or their combinations), their amounts and exposure conditions. In particular, long-term thermal cycling is highly required. Moreover, it is useful to carry out a systematic assessment using the alloys without Pt in order to distinguish the effects caused by Pt and those brought about by other additions.

This paper reports the results of the first step of implementation of such a systematic approach, focused on studying the oxidation behavior under isothermal and long-term (up to 2250 h) thermal cycling conditions of four γ/γ′-type Ni–Al alloys: unmodified, and containing various additions (Hf, combination of Hf and Y, and combination of Hf and Si). The contents of the additions were chosen in order to: (1) investigate the effectiveness of the beneficial effect of reactive elements in terms of lower and higher Hf contents and combined Hf + Y additions, (2) determine whether additions of Si can enhance the oxidation resistance of the alloy containing higher amounts of Hf. The lower content of Hf was chosen taking into account results reported by Gheno et al. [14] in order to meet the so-called Hf-tolerance criterion related to the solubility limit of Hf in the alloy and the propensity to HfO_2 precipitation in the alloy, while higher content exceeded significantly this threshold. The contents of Hf and Y added together were based on the co-doping approach proposed by Pint [24] and investigated more in detail by Kim et al. [18].

Materials and Experimental

Four γ/γ′ Ni-based alloys of the following compositions were manufactured in the form of rods having a diameter of 12 mm and length of 200 mm using conventional vacuum melting: (1) unmodified (referred to as 'γ0'), (2) containing 1.0 wt% of Hf (referred to as 'γHf'), (3) containing a combination of 0.3 wt% of Hf and 0.03 wt% of Y (referred to as 'γHfY'), and (4) containing 1.0 wt% of Hf and 1.0 wt% of Si (referred to as 'γHfSi'). The actual compositions determined using the ICP-OES, Inductively Coupled Plasma—Optical Emission Spectrometry, at Łukasiewicz Research Network, Institute of Non-Ferrous Metals (ŁRN-INFM) in Gliwice, Poland, are collected in Table 1 (the 12.5–13.0 wt% of Al is close to the 22 at.%). The lower content of S than 20 ppmw was assessed also in ŁRN-INFM

using infrared spectral absorption method for all the alloys. The as-cast alloys were vacuum annealed at 1200 °C, for 6 h and subsequently at 1150 °C for 48 h, as proposed elsewhere [5]. The specimens in the form of thin disks of thickness 1 mm were cut from the rods in the direction perpendicular to their longer axis. They were subjected to standard mechanical treatment finished with polishing using 1 μm diamond paste and cleaning and degreasing procedures.

Oxidation exposures were carried out at 1150 °C in ambient, stagnant air, under: (1) isothermal conditions, carried out for 50 h using a thermobalance which enabled continuous monitoring of the weight with an accuracy down to 10^{-6} g (MK2 Vacuum Head Microbalance, CI Electronics Ltd, UK); and (2) thermal-cycling conditions for up to 2225 1-h cycles in air, carried out in a horizontal furnace; each cycle consisted of a 1-h exposure followed by rapid removal of the samples and holding them for 15 min at room temperature. By the end of the latter period, the samples were weighed using a standard analytical balance (accuracy of 10^{-4} g). The net-weight change was followed. During the first 30 cycles, the samples were weighed after each cool-down, over the next 50 cycles, the samples were weighed twice daily, and in the following cycles the samples were weighed once daily.

The starting materials and oxidized samples were subjected to SEM (Scanning Electron Microscopy) observations, EDX (Energy-Dispersive X-ray Spectrometry) analysis of chemical composition and XRD (X-Ray Diffraction) analysis of phase composition using facilities available at Faculty of Material Science and Ceramics AGH-UST. Both the surfaces and polished cross-sections were observed and analyzed using the SEM + EDX approach.

Results

The results of the oxidation runs are shown in Fig. 1 and in Table 2 the parabolic oxidation rate constants are collected together with the ranges of their relevance. The parabolic system of coordinates in the form of $\Delta m/A$ versus $t^{1/2}$ dependence
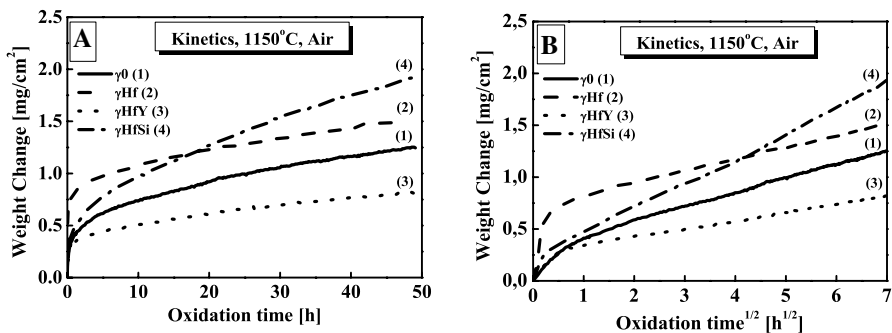
Fig. 1 Oxidation results obtained under isothermal conditions (1150 °C, air): **A** linear plot; **B** parabolic plot

Table 2 Parabolic oxidation rate constants and the corresponding parabolic ranges of kinetics

Alloy	Parabolic range (h)	k_p ($g^2 cm^{-4} s^{-1}$)
γ0	4–50	$5.0 \cdot 10^{-12}$
γHf	1–50	$3.5 \cdot 10^{-12}$
γHfY	1–50	$1.7 \cdot 10^{-12}$
γHfSi	0.25–50	$1.6 \cdot 10^{-11}$

was applied, as the best suitable for interpretation of the kinetic results, if the initial stages should also be followed, as indicated elsewhere [25–27].

The course of the oxidation kinetic runs in all cases can be divided into two consecutive stages: (1) transient, and (2) steady-state parabolic. As it follows from Table 2, the duration of the transient stages was different for the various alloys, the shortest (0.25 h) being for γHfSi and the longest-lasting (4 h) for γ0. It took 1 h for the two other alloys. Moreover, the transient stages resulted in different weight gains from which the steady-state scale growth occurred obeying the parabolic rate law (stage 2). In Table 3 the weight gains corresponding to the transition between the transient and steady-state parabolic stages are collected. Those relevant to the entire exposures (50 h) are also shown in order to enable the effects related to the transient and parabolic oxidation stages to be distinguished. As can be seen from Table 3, a significant contribution of the transient stages to the overall weight gain was observed for the γHf and γ0 alloys.
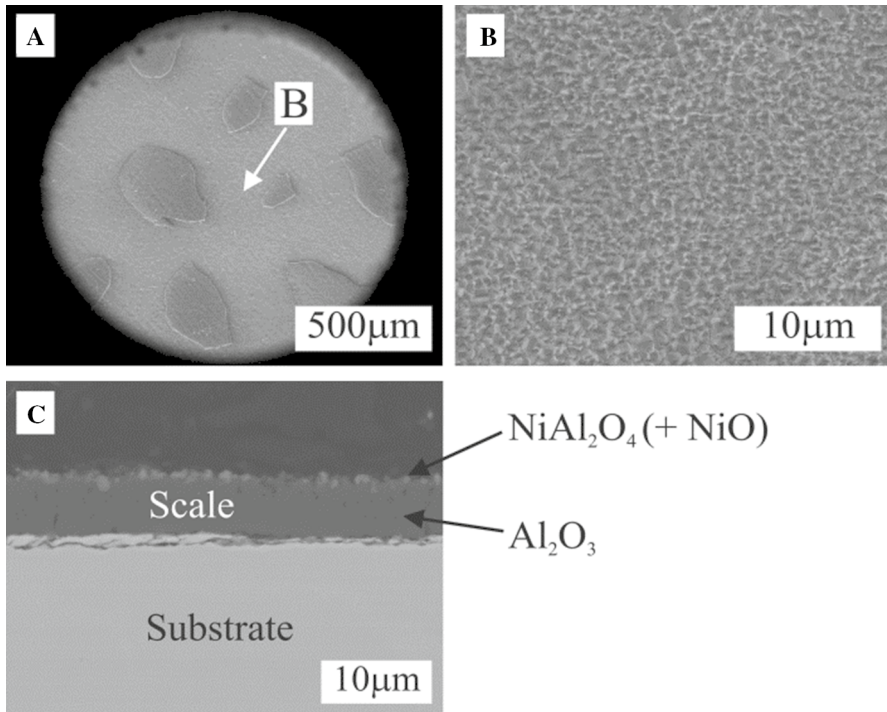
The parabolic oxidation rate constants corresponding to the steady-state oxidation were the lowest for γHfY alloy, slightly higher for the γHf and γ0 alloys, ~ 2 and ~ 3 times, respectively, and much higher, by one order of magnitude, for γHfSi alloy.

Figures 2, 3, 4 and 5 show the SEM images of the surface (low and high magnifications) and polished cross-sections of the samples oxidized under isothermal conditions, with descriptions of the phases and enrichments based on the XRD and EDX results. From Figs. 2A and 5A, B it follows that local spallation of the scales to bare substrates occurred on the γ0 and γHfSi alloys during cooling from the reaction temperature to room temperature. Moreover, for alloy γHfSi it appears from comparison of Fig. 1 (the largest weight gains) and Fig. 5 (the thinnest scale without Ni-rich outermost layer) that spallation of the outermost layer comprising the fastest-growing Ni-oxide occurred.

The following can be inferred from Figs. 2, 3, 4 and 5 and the results of the XRD + EDX analyses:

Table 3 Weight gains corresponding to the initial stages of isothermal oxidation prior to the parabolic growth of the protective scale (last column: weight gains after exposure for 50 h, the entire duration of the exposure)

Material	t (h)	$\Delta m/S$ (mg/cm^2)	Total $\Delta m/S$ (mg/cm^2)
γ0	4	0.6	1.25
γHf	1	0.8	1.5
γHfY	1	0.35	0.8
γHfSi	0.25	0.4	1.9

Fig. 2 SEM images of surface (**A**, **B**) and polished cross- section (**C**) of γ0 alloy oxidized under isothermal conditions (1150 °C, air, 50 h) with adherent scale and spalled regions

1. the relative thicknesses of the scales were consistent with the kinetic data (Fig. 1) for all alloys, except for alloy γHfSi;
2. in all cases, multi-layer scales developed consisting of (starting from the interface scale-underlying substrate) a thicker in the case of γ0 alloy and much thinner and irregular on all the Hf-containing alloys thin protective α-Al$_2$O$_3$ layer, a layer of NiAl$_2$O$_4$ spinel and on the γHf and γHfY alloys an outermost scale layer consisting of NiO (NiO on γ0 was not found as a continuous layer but some EDX results at certain points suggested the local presence of this oxide);
3. the NiO outermost scale layer consisting of blocky grains that developed on the γHf alloy was fairly thick;
4. Hf-rich oxide precipitates were found in substrates and scales after oxidation of all the Hf-containing alloys;
5. the size and distribution of Hf-rich oxides depended on the alloy—the largest were observed in the case of γHf alloy, and the finest on γHfY alloy;
6. Hf-rich oxide precipitates were found only in the innermost scale layer (α-Al$_2$O$_3$) and at the α-Al$_2$O$_3$/NiAl$_2$O$_4$ interface, exhibiting more or less continuous band-type structure in the latter case;
7. the thickness of the surface layer of the substrate containing Hf-rich precipitates was the lowest in oxidized γHfSi alloy (~ 5 μm), while higher and comparable (~ 8 μm) in oxidized γHf and γHfY alloys.
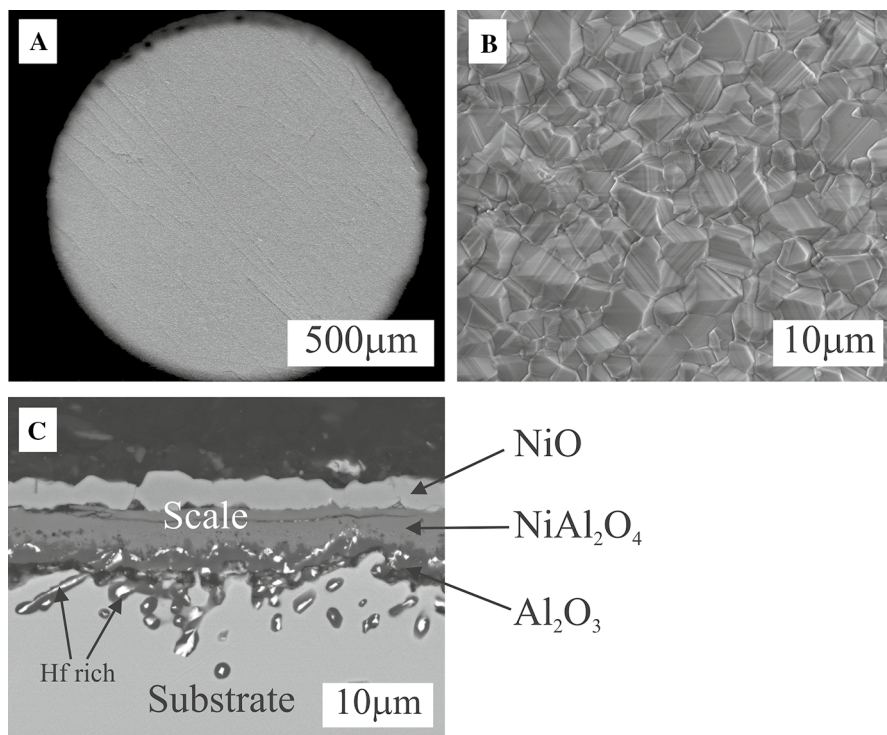
Fig. 3 SEM images of surface (**A**, **B**) and polished cross-section (**C**) of γHf alloy oxidized under isothermal conditions (1150 °C, air, 50 h)

The thermal cycling results are shown in Fig. 6 in terms of two plots relevant to the entire exposure period (Fig. 6A) and to the initial 50 cycles (Fig. 6B). They demonstrate that: (1) Only a few cycles were required to observe a negative weight change in the unmodified alloy; (2) all the additions resulted in a shift of the weight loss to a longer exposure time corresponding to improved oxidation resistance; (3) only in the case of the combination of Hf + Y did the additions bring about a relatively good long-term oxidation resistance which manifests itself in a positive weight gain even after 2225 thermal cycles, which is not the case for all the other alloys; (4) the beneficial effect of Hf + Si additions was noticeable but not rather short-term one (after less than 20 cycles a negative weight change was observed), while that of Hf addition was much more durable (a negative weight change after more than 500 cycles).

Figures 7, 8, 9 and 10 show the SEM images of the surface (low and high magnifications) and polished cross sections of the samples oxidized under thermal-cycling conditions, with descriptions of the phases and enrichments based on the XRD and EDX results. From all the figures, it follows that the scales were multilayered and non-uniform, resembling more or less the structures observed under isothermal conditions. They also reflected the locally occurring sequential
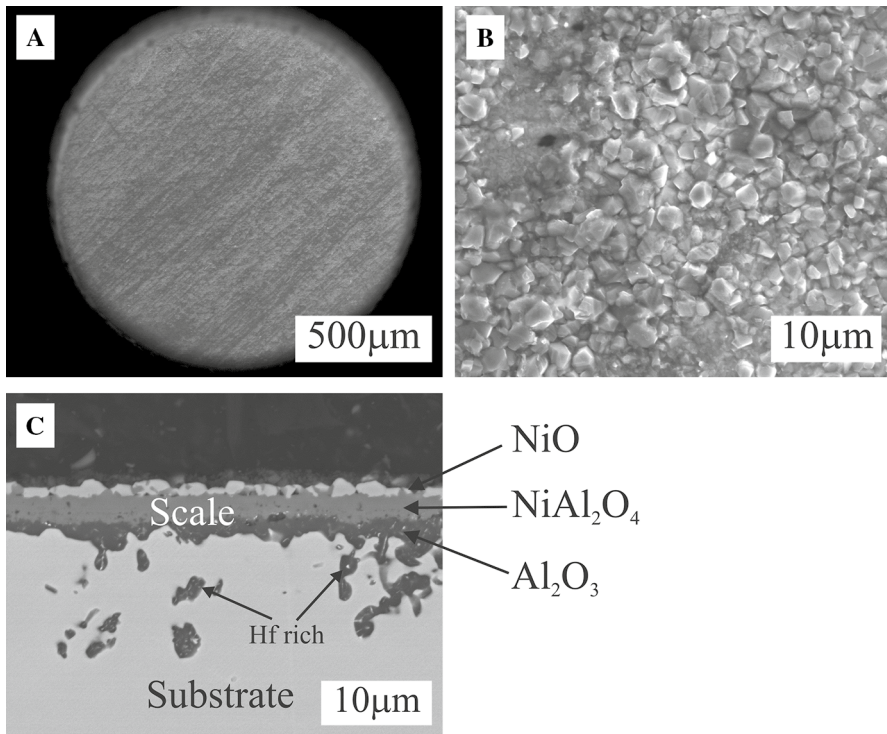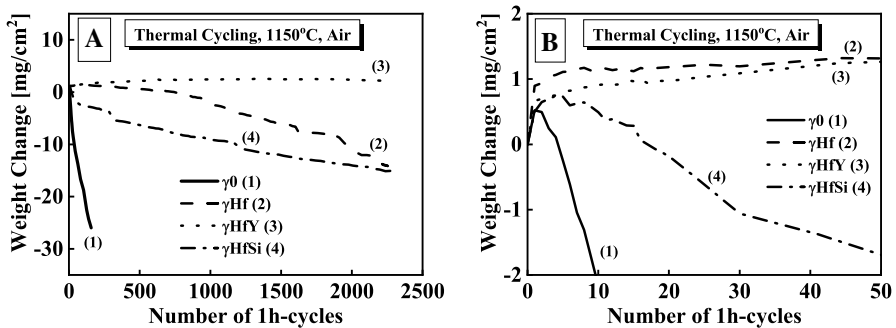
Fig. 4 SEM images of surface (**A**, **B**) and polished cross-section (**C**) of γHfY alloy oxidized under isothermal conditions (1150 °C, air, 50 h)

process comprising scale growth:spallation:re-growth cycles. Only in the case of the alloy γHfY three conditions were simultaneously fulfilled: (1) a relatively thick α-Al_2O_3 protective layer; (2) no large Hf-rich precipitates at or close to the scale–substrate interface and in the substrate, and (3) no thick NiO outermost scale layer. Large Hf-rich oxide precipitates, being HfO_2 (according to the XRD results), were found in the substrate and in the scale in the case of the γHf and γHfSi alloys, while very thick Ni-containing layers were found on the γ0 alloy. From the XRD analysis, it follows that in the case of the scale on the γHfY alloy, Hf was present in the form of Hf-containing oxide precipitates, identified as HfO_2 and/or $Y_2Hf_2O_7$. They were rather uniformly distributed across the α-Al_2O_3 layer and in the $NiAl_2O_4$ spinel layer, but rather close to the α-alumina/(Ni–Al)-spinel interface. The $Y_2Hf_2O_7$ oxide was the only oxide form of Y found in both the scale and the substrate.

Figures 7, 8, 9 and 10 show the SEM images of the surface (low and high magnifications) and polished cross sections of the samples oxidized under thermal-cycling conditions, with descriptions of the phases and enrichments based on the XRD and EDX results. From all the figures, it follows that the scales were multilayered and non-uniform, resembling more or less the structures observed
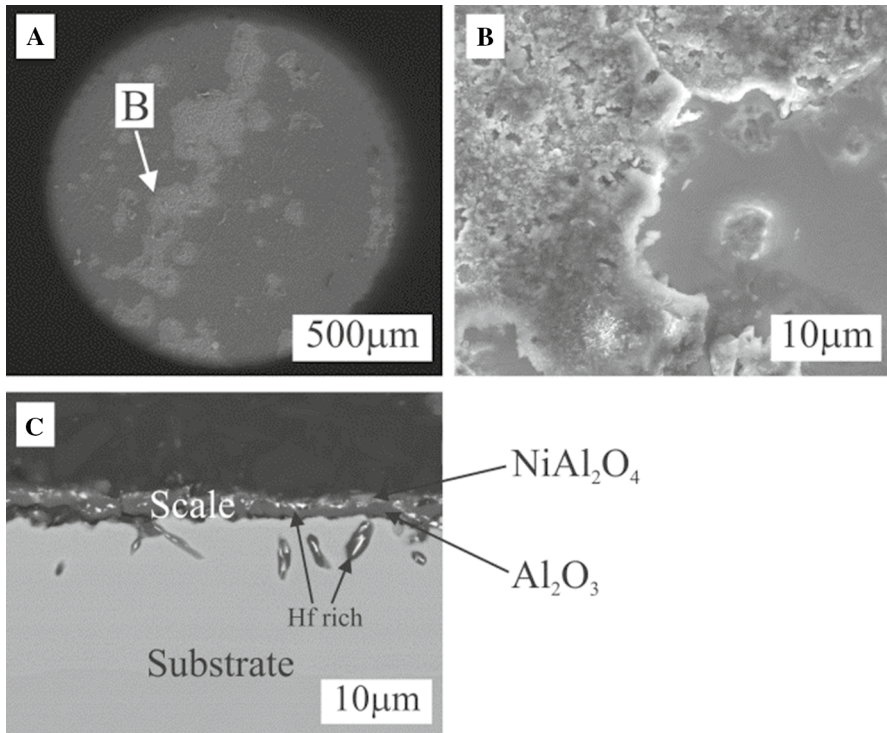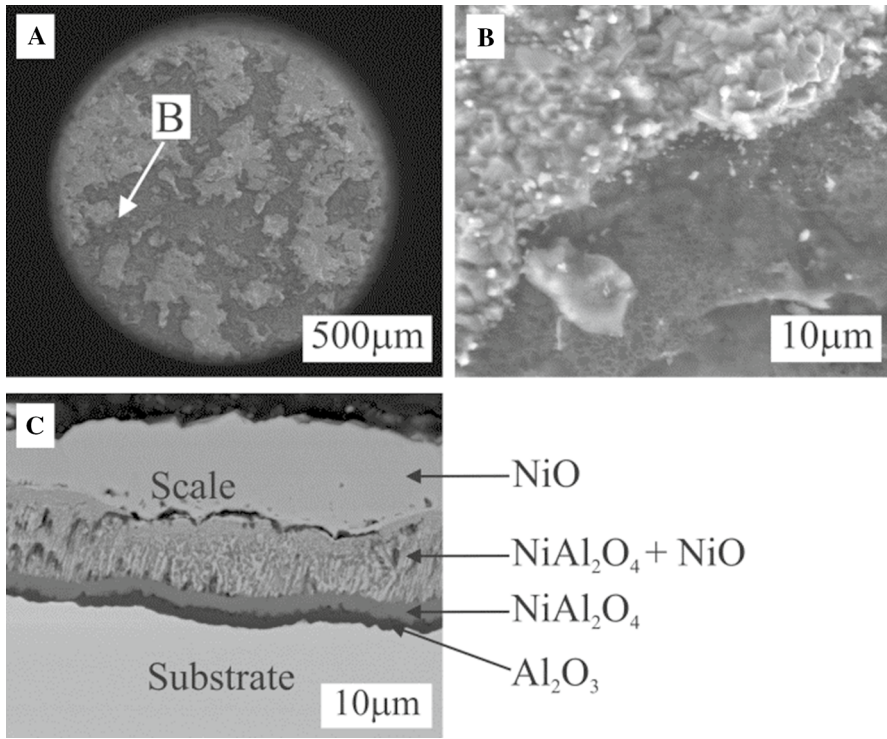
Fig. 5 SEM images of surface (**A**, **B**) and polished cross-section (**C**) of γHfSi alloy oxidized under isothermal conditions (1150 °C, air, 50 h)

Fig. 6 Oxidation results obtained under thermal-cycling conditions (1150 °C, air): **A** full range of cycles; **B** initial 50 cycles

under isothermal conditions. They also reflected the locally occurring sequential process comprising scale growth:spallation:re-growth cycles. Only in the case of the alloy γHfY three conditions were simultaneously fulfilled: (1) a relatively thick α-Al_2O_3 protective layer; (2) no large Hf-rich precipitates at or close to the
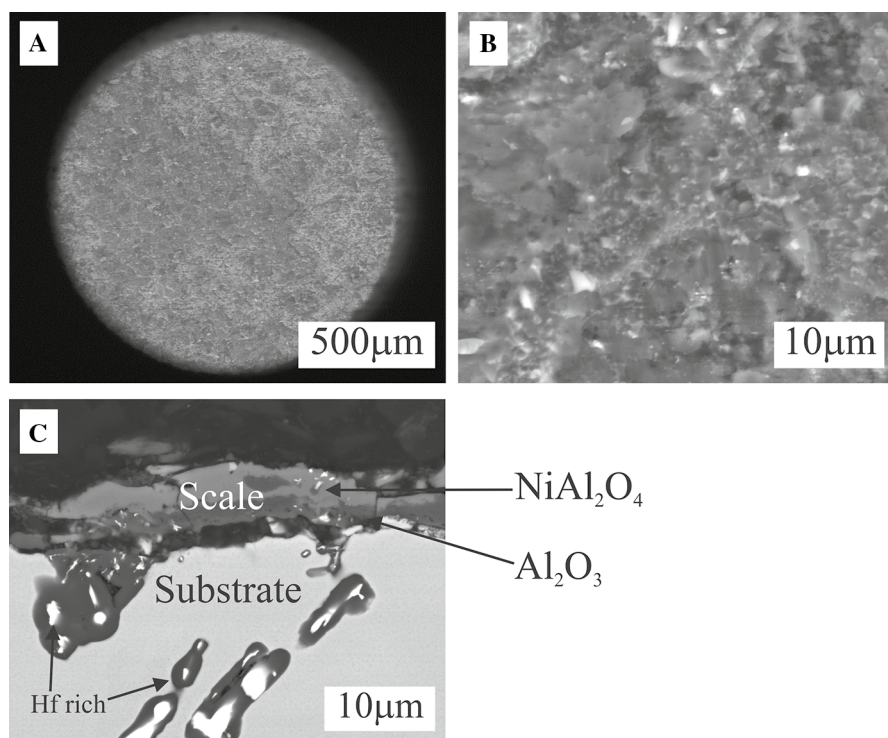
Fig. 7 SEM images of surface (**A**, **B**) and polished cross-section (**C**) of γ0 alloy oxidized under thermal-cycling conditions (1150 °C, air, 150 1-h cycles)

scale–substrate interface and in the substrate, and (3) no thick NiO outermost scale layer. Large Hf-rich oxide precipitates, being HfO_2 (according to the XRD results), were found in the substrate and in the scale in the case of the γHf and γHfSi alloys, while very thick Ni-containing layers were found on the γ0 alloy. From the XRD analysis it follows that in the case of the scale on the γHfY alloy, Hf was present in the form of Hf-containing oxide precipitates, identified as HfO_2 and/or $Y_2Hf_2O_7$. They were rather uniformly distributed across the α-Al_2O_3 layer and in the $NiAl_2O_4$ spinel layer, but rather close to the α-alumina/(Ni–Al)-spinel interface. The $Y_2Hf_2O_7$ oxide was the only oxide form of Y found in both the scale and the substrate.

It should be noted that thermal cycling and the subsequent preparation procedure of the polished cross sections might bring about the spallation of parts of the scale, which could prevent the scale's outermost layers from being found through observations of the cross-sections. Therefore, it should be added that the XRD analysis carried out from the surface of samples prior to the cross-section preparation exhibited: (1) no evidence of NiO in scales on the thermally cycled alloys γHf and γHfY; (2) the presence of NiO in scales on the thermally cycled alloys γ0 and γHfSi; (3) evidence of small peaks corresponding to SiO_2 in scale on the thermally cycled γHfSi.
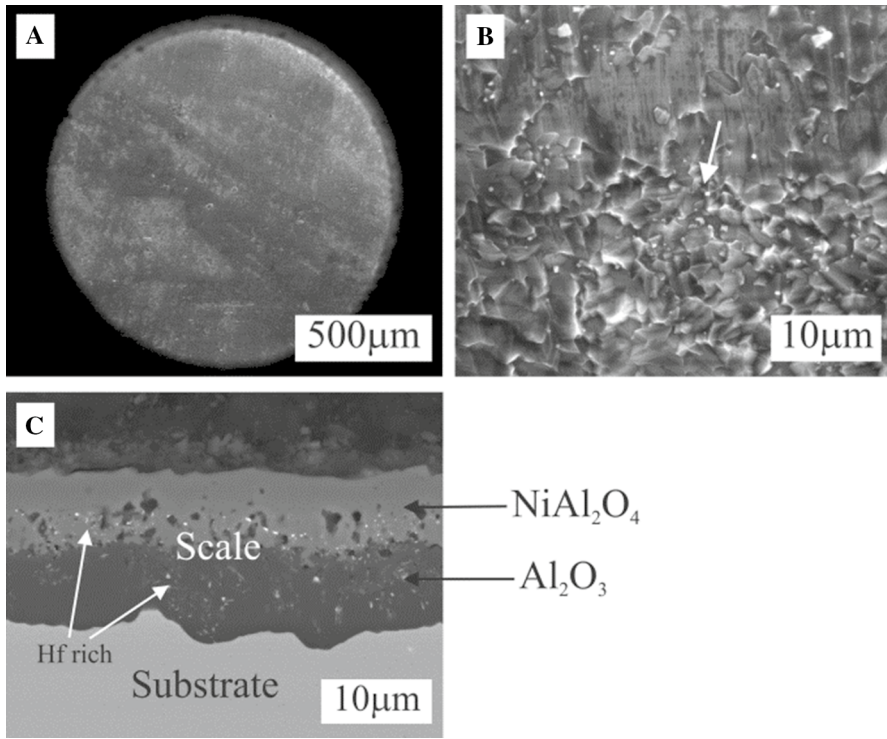
Fig. 8 SEM images of surface (**A**, **B**) and polished cross-section (**C**) of γHf alloy oxidized under thermal-cycling conditions (1150 °C, air, 2225 1-h cycles)

Discussion

The isothermal and thermal cycling exposures led to consistent results concerning the determination of the best oxidation-resistant alloy among the four studied γ/γ′ Ni-based ones. With respect to both of the commonly applied factors: (1) the scale growth rate upon isothermal exposure, and (2) the shape of the weight change versus number of thermal cycles curve, the behavior of the alloy containing a combination of (Hf + Y) additions was superior to all the other alloys. It exhibited the lowest parabolic oxidation rate constant (Fig. 1, Table 2) and was the only alloy for which only positive weight changes, indicating no extensive spallation, were found during long-term thermal cycling, for up to 2225 cycles (Fig. 2).

The more detailed discussion of the oxidation behavior of the studied alloys requires the following interrelated issues to be taken into account: (1) quantitative interpretation of the oxidation kinetics, involving transient oxidation, which precedes the steady state, the protective stage of this process; (2) the composition and structure of the scale; and (3) addition-related effects, including their distribution in the scale and in the substrate.

Fig. 9 SEM images of surface (**A**, **B**) and polished cross- section (**C**) of γHfY alloy oxidized under thermal-cycling conditions (1150 °C, air, 2225 1-h cycles)

The importance of the transient oxidation is associated with the initial formation of fast-growing non-protective oxides.

Two parameters should be used to quantify these stages: (1) their duration, and (2) the resulting overall weight gain. Both factors, collected in Table 3, are significant for the following two reasons: (1) Thermal-cycling experiments usually rely on a short duration individual cycle (of the order of one hour), and it is worth knowing which scale, transient or protective, is subjected to the first cycles; (2) the thermal stresses generated during temperature changes, which result frequently in accelerated degradation of materials, depend on the overall thickness of the scale. It can be inferred from Table 3 that: (1) the shortest transient oxidation occurred in the case of the alloy containing (Hf + Si) additions (0.25 h), the intermediate in the case of Hf-containing and (Hf + Y)-containing alloys (1 h), and the longest in the case of the unmodified alloy (4 h); (2) the highest weight gain during transient oxidation was observed for the Hf-containing alloy (0.8 mg/ cm^2), slightly lower for unmodified alloy (0.6 mg/cm^2), but after 4 h, and the lowest—and comparable—for alloys containing (Hf + Y) and (Hf + Si) (0.35 mg/ cm^2 and 0.4 mg/cm^2, respectively, but after different oxidation periods of 1 h and 0.25 h, respectively). It should be noted that for the duration of the first thermal
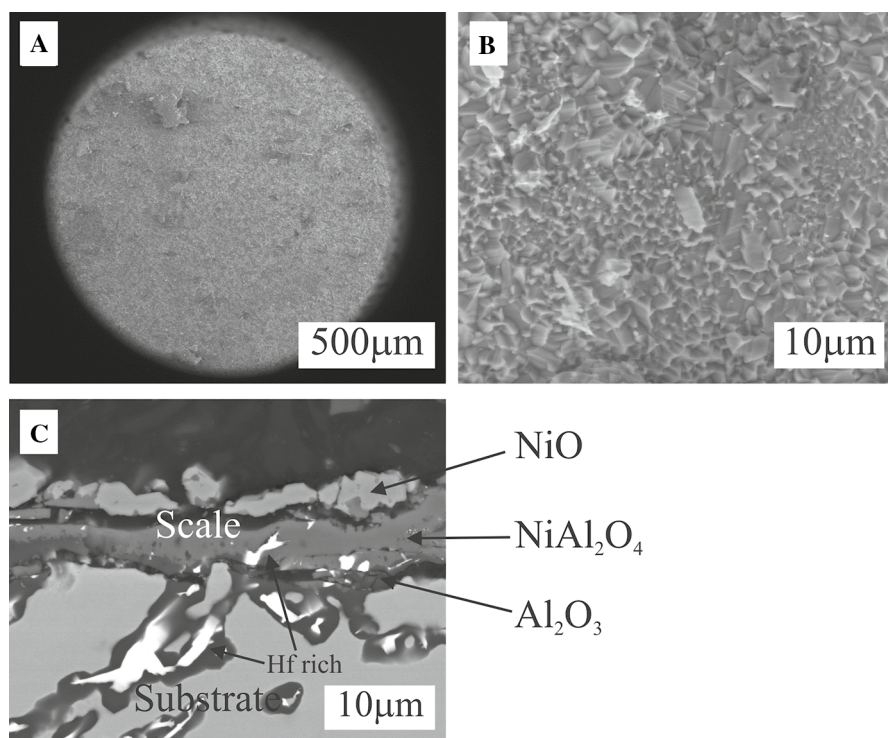
Fig. 10 SEM images of surface (**A**, **B**) and polished cross-section (**C**) of γHfSi alloy oxidized under thermal-cycling conditions (1150 °C, air, 2225 1-h cycles)

cycle, 1 h, the weight gain of the unmodified alloy was 0.4 mg/cm^2 and for that containing (Hf + Si) it was 0.45 mg/cm^2. However, the transient growth stage was relevant to the unmodified alloy and the steady-state stage to the alloy containing (Hf + Si).

It may follow from the above discussion that the scales on alloys γ0 and γHf were unfavorable in terms of subjecting them to thermal cycling with respect to their stage of development or thickness, respectively. However, the thermal cycling results (Fig. 6) indicated that this inference is an oversimplification.

The subsequent stage of the scale growth, the steady-state one, obeyed the parabolic rate law: $(\Delta m/A)^2 = k_p t$, and comparison of the rate constant (k_p) values (Table 2) indicates that this stage, referred to as the protective one, occurs much faster for γHfSi alloy than for the other alloys. The slowest growth rate, with the k_p one order of magnitude smaller than in the case of γHfSi, was found for γHfY alloy.

As a result of both stages, transient and steady-state, the overall weight gain during isothermal exposure (50 h) was the lowest in the case of γHfY alloy and the highest in the case of γHfSi (Fig. 2 and Table 3). That in the case of γHf alloy was significantly higher than found for γHfY alloy, but slightly lower than for γHfSi alloy.

Concerning the composition and structure of the scale, it should be noted that in all cases multi-layered scales were formed. Their structure and composition depended on both the alloy composition and the exposure conditions (Figs. 2, 3, 4, 5, 7, 8, 9, 10). However, also in all cases, the α-Al_2O_3 protective layer was observed at the scale–substrate interface. On all the Hf-containing alloys oxidized under isothermal conditions, it was relatively thin.

Oxidation of the γHf and γHfSi alloys resulted in large Hf-containing oxides that penetrated into the underlying alloy or formed internal oxide precipitates in the surface layer of these substrates. Hf-containing oxide precipitates were also observed in the scale, but rather within the α-Al_2O_3 and at or close to its interface with the $NiAl_2O_4$ spinel layer.

The most spectacular difference between the scales structure on the most resistant alloy (γHfY) and the other ones was observed on thermally cycled samples. In the former case, a relatively thick and regular α-Al_2O_3 innermost layer was formed with fairly fine and uniformly distributed Hf-rich oxide particles, above which the $NiAl_2O_4$ layer developed (Fig. 9). Moreover, no Hf-rich oxide protrusions into the substrate and/or internal oxide particles were found. In contrast, on both the other Hf-containing alloys, the innermost layer of α-Al_2O_3 was thin and highly irregular, not necessarily continuous and contained large Hf-rich oxide precipitates (Figs. 8, 10). Moreover, large Hf-containing protrusions into the underlying substrates as well as precipitates within the scale were formed.

It can thus be inferred that the scales observed on the two latter alloys after their thermal cycling developed through a repeated sequence of scale growth, spallation and re-growth processes, which is consistent with the thermal cycling results shown in Fig. 6. However, it should be emphasized that all the additions improved the oxidation resistance of the reference alloy under thermal cycling conditions.

It should be noted that, both qualitatively and quantitatively, the results obtained are consistent with those reported by other authors in terms of the following: (1) The k_p values of Si-containing alloy were close to that observed for Ni15Cr5Al + Si (1 wt%) [17]; (2) Si additions resulted in reaching the steady-state oxidation earlier (shortened transient oxidation stages) [17]; (3) Hf additions, if exceeding the solubility limit (over-doping), form oxide precipitates in the underlying substrates as well as in the scales [6, 7, 14, 15, 19]. Comparison of the results obtained with those in an extensive study of the effect of Hf, Y and Si additions on the oxidation behavior of Ni20Al5Cr alloy and René N5 superalloy reported elsewhere [11] led to some discrepancies that need further investigation involving the effect of Cr and the content of the additions.

The premise based on the results reported here and on references is that lower amounts of Hf addition should be more extensively tested also for Hf applied together with Y-additions and taking into account the co-doping effects related to other elements such as Pt and Cr. The ongoing research is also directed toward elucidation of the mechanisms of: the early oxidation stages and of the possibility of further improvement of the oxidation resistance through the application of surface layers of Pt, Al, Cr and/or Al_2O_3 and getting better insight into degradation mechanisms of γ/γ'-type Ni–Al alloys.

Concluding Remarks

Investigation of the oxidation behavior under isothermal and thermal cycling conditions at 1150 °C, in air, of four γ/γ′-type Ni–Al alloys: unmodified, containing 1.0 wt% of Hf, containing a combination of 0.3 wt% of Hf and 0.03 wt% of Y, and containing 1.0 wt% of Hf and 1.0 wt% of Si, enabled the following conclusions to be inferred:

1. All three types of additions resulted in improved oxidation behavior of the studied γ/γ′ Ni-based alloys, but only that of (Hf + Y) brought about a long-term effect of interest with respect to further applications.
2. Complex, multi-layered scales developed in all cases, consisting of an innermost layer of α-Al_2O_3, a $NiAl_2O_4$-spinel layer (outer or intermediate, depending on the number of layers) and, sometimes, an outermost scale layer composed of NiO.
3. Two stages, transient oxidation and steady-state oxidation, were observed, with the duration of the transient stages being strongly dependent on the alloy and with markedly different weight gains at the end of the transient stages.
4. The oxidation rate during the steady-state oxidation stages was the highest in the case of (Hf + Si)-containing alloy and the slowest for (Hf + Y)-containing alloy.
5. Large Hf-rich oxide protrusions into the underlying substrate and in the scale developed on the less oxidation-resistant materials containing Hf amounts exceeding its solubility limit in the alloy due to the so-called over-doping effect. In the case of (Hf + Y)-containing alloy, they initially formed but later either disappeared (protrusions) or formed fine and uniformly distributed precipitates in the scale.
6. The contents of the additions need further modifications toward optimizing the oxidation resistance. However, the combined incorporation of Hf and Y at applied levels is a promising starting point for future work.

References

1. T. Pollock and S. Tin, *Journal of Propulsion and Power* **22**, 2006 (361).
2. B. Gleeson, *Journal of Propulsion and Power* **22**, 2006 (375).
3. B. A. Pint, *Surface and Coatings Technology* **188–189**, 2004 (71).
4. B. Gleeson, W. Wang, S. Hayashi, and D. Sordelet, *Materials Science Forum* **461–464**, 2004 (213).
5. S. Hayashi, T. Narita, and B. Gleeson, *Materials Science Forum* **522–523**, 2006 (229).
6. T. Izumi, N. Mu, L. Zhang, and B. Gleeson, *Surface and Coatings Technology* **202**, 2007 (628).
7. N. Mu, T. Izumi, L. Zhang, and B. Gleeson, in *Superalloys 2008*, eds. R. C. Reed, K. A. Green, P. Carron, T. P. Gabb, M. G. Fahrmann, E. S. Huron, and S. A. Woodard, p. 629.
8. B. A. Pint, J. A. Haynes, K. L. More, J. H. Schneibel, Y. Zhang, and I. G. Wright, in *Superalloys 2008*, eds. R. C. Reed, K. A. Green, P. Carron, T. P. Gabb, M. G. Fahrmann, E. S. Huron, and S. A. Woodard, p. 641.
9. J. A. Haynes, B. A. Pint, Y. Zhang, and I. G. Wright, *Surface and Coatings Technology* **204**, 2009 (816).
10. Y. Zhang, S. Li, and Y. Han, *Rare Metals* **30**, 2011 (538).
11. Z. Li, *Investigation of the minor-element effects on the oxidation behaviour of γ-Ni+γ′-Ni₃Al alloys*, Ph.D. thesis, University of Pittsburgh, 2014.
12. H. M. Tawancy, L. M. Al-Hadhrami, A. I. Mohammed, F. K. Alyousef, and H. Dafalla, *Oxidation of Metals* **83**, 2015 (417).
13. J. He, Z. Zhang, H. Peng, S. Gong, and H. Guo, *Corrosion Science* **98**, 2015 (699).
14. T. Gheno, B.-C. Zhou, A. Ross, X. Liu, G. Lindwall, Z.-K. Liu, and B. Gleeson, *Oxidation of Metals* **87**, 2017 (297).
15. R. Swadźba, *Prace Instytutu Metalurgii Żelaza* **70**, 2018 (19).
16. W.-T. Chen, B. Gleeson, and A. Heuer, *Oxidation of Metals* **92**, 2019 (137).
17. E. Wang, D. J. Sun, H. Liu, M. Lu, W. Guo, B. Zheng, and X. Zhang, *Oxidation of Metals* **92**, 2019 (151).
18. D. E. Kim, S.-L. Shang, Z. Li, B. Gleeson, and Z.-K. Liu, *Oxidation of Metals* **92**, 2019 (303).
19. X. Cao, J. He, H. Chen, B. Zhou, L. Liu, and H. Guo, *Corrosion Science* **167**, 2020 (108481).
20. Y. F. Yang, P. Ren, Z. B. Bao, S. L. Zhu, F. H. Wang, and W. Li, *Journal of Materials Science* **55**, 2020 (11687).
21. J. Jedliński, *Solid State Phenomena* **21 & 22**, 335–390 (1992).
22. P. Y. Hou, *Materials Science Forum* **696**, 2011 (39).
23. D. Naumenko, B. A. Pint, and W. J. Quadakkers, *Oxidation of Metals* **64**, 2016 (397).
24. B. A. Pint, *Journal of the American Ceramic Society* **86**, 2003 (686).
25. D. Monceau and B. Pieraggi, *Oxidation of Metals* **50**, 1998 (477).
26. W. J. Quadakkers, D. Naumenko, E. Wessel, V. Kobuchey, and L. Singheiser, *Oxidation of Metals* **61**, 2004 (17).
27. B. Pieraggi, *Oxidation of Metals* **64**, 2005 (397).

Authors and Affiliations

Jarosław Dąbek[1] · Janusz Prażuch[1] · Monika Migdalska[1] · Monika Jawańska[1] · Magdalena Ziąbka[1] · Monika Wójcik-Bania[2] · Jerzy Jedliński[1]

Jarosław Dąbek
dabek@agh.edu.pl

Janusz Prażuch
prazuch@agh.edu.pl

Monika Migdalska
mmska@agh.edu.pl

Monika Jawańska
jawanska@agh.edu.pl

Magdalena Ziąbka
ziabka@agh.edu.pl

Monika Wójcik-Bania
wojcikm@agh.edu.pl

[1]   Faculty of Materials Science and Ceramics, AGH University of Science and Technology, al. Mickiewicza 30, 30-059 Kraków, Poland

[2]   Faculty of Geology, Geophysics and Environmental Protection, AGH University of Science and Technology, al. Mickiewicza 30, 30-059 Kraków, Poland